First Measurement of θ_{13} From Delayed Neutron Capture on Hydrogen in the Double Chooz Experiment

Y. Abe[ac], C. Aberle[u], J.C. dos Anjos[e], J.C. Barriere[o], M. Bergevin[i], A. Bernstein[p], T.J.C. Bezerra[aa], L. Bezrukhov[n], E. Blucher[f], N.S. Bowden[p], C. Buck[u], J. Busenitz[b], A. Cabrera[d], E. Caden[j], L. Camilleri[h], R. Carr[h], M. Cerrada[g], P.-J. Chang[q], P. Chimenti[ag], T. Classen[i,p], A.P. Collin[o], E. Conover[f], J.M. Conrad[t], J.I. Crespo-Anadón[g], K. Crum[f], A. Cucoanes[y], E. Damon[j], J.V. Dawson[d,ai], S. Dazeley[p], D. Dietrich[af], Z. Djurcic[c], M. Dracos[x], V. Durand[o,d], J. Ebert[k], Y. Efremenko[z], M. Elnimr[y], A. Erickson[p], A. Etenko[s], M. Fallot[y], M. Fechner[o], F. von Feilitzsch[ae], J. Felde[i], S.M. Fernandes[b], V. Fischer[o], D. Franco[d], A.J. Franke[h], M. Franke[ae], H. Furuta[aa], R. Gama[e], I. Gil-Botella[g], L. Giot[y], M. Göger-Neff[ae], L.F.G. Gonzalez[ah], L. Goodenough[c], M.C. Goodman[c], J.TM. Goon[b], D. Greiner[af], N. Haag[ae], S. Habib[b], C. Hagner[k], T. Hara[r], F.X. Hartmann[u], J. Haser[u], A. Hatzikoutelis[z], T. Hayakawa[v], M. Hofmann[ae], G.A. Horton-Smith[q], A. Hourlier[d], M. Ishitsuka[ac], J. Jochum[af], C. Jollet[x], C.L. Jones[t], F. Kaether[u], L.N. Kalousis[aj], Y. Kamyshkov[z], D.M. Kaplan[m], T. Kawasaki[v], G. Keefer[p], E. Kemp[ah], H. de Kerret[d,ai], T. Konno[ac], D. Kryn[d], M. Kuze[ac], T. Lachenmaier[af], C.E. Lane[j], C. Langbrandtner[u], T. Lasserre[o,d], A. Letourneau[o], D. Lhuillier[o], H.P. Lima Jr[e], M. Lindner[u], J.M. López-Castaño[g], J.M. LoSecco[w], B.K. Lubsandorzhiev[n], S. Lucht[a], D. McKee[q], J. Maeda[ad], C.N. Maesano[i], C. Mariani[aj], J. Maricic[j], J. Martino[y], T. Matsubara[ad], G. Mention[o], A. Meregaglia[x], M. Meyer[k], T. Miletic[j], R. Milincic[j], H. Miyata[v], Th.A. Mueller[aa], Y. Nagasaka[l], K. Nakajima[v], P. Novella[g], M. Obolensky[d], L. Oberauer[ae], A. Onillon[y], A. Osborn[z], I. Ostrovskiy[b], C. Palomares[g], I.M. Pepe[e], S. Perasso[j], P. Perrin[o], P. Pfahler[ae], A. Porta[y], W. Potzel[ae], G. Pronost[y], J. Reichenbacher[b], B. Reinhold[u], A. Remoto[y,d], M. Röhling[af], R. Roncin[d], S. Roth[a], B. Rybolt[z], Y. Sakamoto[ab], R. Santorelli[g], F. Sato[ad], S. Schönert[ae], S. Schoppmann[a], T. Schwetz[u], M.H. Shaevitz[h], S. Shimojima[ad], D. Shrestha[q], J-L. Sida[o], V. Sinev[n,o], M. Skorokhvatov[s], E. Smith[j], J. Spitz[t], A. Stahl[a], I. Stancu[b], L.F.F. Stokes[af], M. Strait[f], A. Stüken[a], F. Suekane[aa], S. Sukhotin[s], T. Sumiyoshi[ad], Y. Sun[b], R. Svoboda[i], K. Terao[t], A. Tonazzo[d], M. Toups[h], H.H. Trinh Thi[ae], G. Valdiviesso[e], C. Veyssiere[o], S. Wagner[u], H. Watanabe[u], B. White[z], C. Wiebusch[a], L. Winslow[t], M. Worcester[f], M. Wurm[k], F. Yermia[y], V. Zimmer[ae]

[a]III. Physikalisches Institut, RWTH Aachen University, 52056 Aachen, Germany
[b]Department of Physics and Astronomy, University of Alabama, Tuscaloosa, Alabama 35487, USA
[c]Argonne National Laboratory, Argonne, Illinois 60439, USA
[d]APC, AstroParticule et Cosmologie, Université Paris Diderot, CNRS/IN2P3, CEA/IRFU, Observatoire de Paris, Sorbonne Paris Cité, 75205 Paris Cedex 13, France
[e]Centro Brasileiro de Pesquisas Físicas, Rio de Janeiro, RJ, cep 22290-180, Brazil
[f]The Enrico Fermi Institute, The University of Chicago, Chicago, IL 60637, USA
[g]Centro de Investigaciones Energéticas, Medioambientales y Tecnológicas, CIEMAT, E-28040, Madrid, Spain
[h]Columbia University; New York, NY 10027, USA
[i]University of California, Davis, CA-95616-8677, USA
[j]Physics Department, Drexel University, Philadelphia, Pennsylvania 19104, USA
[k]Institut für Experimentalphysik, Universität Hamburg, 22761 Hamburg, Germany
[l]Hiroshima Institute of Technology, Hiroshima, 731-5193, Japan
[m]Department of Physics, Illinois Institute of Technology, Chicago, Illinois 60616, USA
[n]Institute of Nuclear Research of the Russian Aacademy of Science, Russia
[o]Commissariat à l'Energie Atomique et aux Energies Alternatives, Centre de Saclay, IRFU, 91191 Gif-sur-Yvette, France
[p]Lawrence Livermore National Laboratory, Livermore, CA 94550, USA
[q]Department of Physics, Kansas State University, Manhattan, Kansas 66506, USA
[r]Department of Physics, Kobe University, Kobe, 657-8501, Japan
[s]NRC Kurchatov Institute, 123182 Moscow, Russia
[t]Massachusetts Institute of Technology; Cambridge, MA 02139, USA
[u]Max-Planck-Institut für Kernphysik, 69117 Heidelberg, Germany
[v]Department of Physics, Niigata University, Niigata, 950-2181, Japan
[w]University of Notre Dame, Notre Dame, IN 46556- 5670, USA
[x]IPHC, Université de Strasbourg, CNRS/IN2P3, F- 67037 Strasbourg, France
[y]SUBATECH, CNRS/IN2P3, Université de Nantes, Ecole des Mines de Nantes, F-44307 Nantes, France
[z]Department of Physics and Astronomy, University of Tennessee, Knoxville, Tennessee 37996, USA
[aa]Research Center for Neutrino Science, Tohoku University, Sendai 980-8578, Japan
[ab]Tohoku Gakuin University, Sendai, 981-3193, Japan
[ac]Department of Physics, Tokyo Institute of Technology, Tokyo, 152-8551, Japan
[ad]Department of Physics, Tokyo Metropolitan University, Tokyo, 192-0397, Japan
[ae]Physik Department, Technische Universität München, 85747 Garching, Germany
[af]Kepler Center for Astro and Particle Physics, Universität Tübingen, 72076, Tübingen, Germany
[ag]Universidade Federal do ABC, UFABC, São Paulo, Santo André, SP, Brazil
[ah]Universidade Estadual de Campinas-UNICAMP, Campinas, SP, Brazil
[ai]Laboratoire Neutrino de Champagne Ardenne, domaine d'Aviette, 08600 Rancennes, France
[aj]Center for Neutrino Physics, Virginia Tech, Blacksburg, VA

arXiv:1301.2948v2 [hep-ex] 29 Aug 2013

Abstract

The Double Chooz experiment has determined the value of the neutrino oscillation parameter θ_{13} from an analysis of inverse beta decay interactions with neutron capture on hydrogen. This analysis uses a three times larger fiducial volume than the standard Double Chooz assessment, which is restricted to a region doped with gadolinium (Gd), yielding an exposure of 113.1 GW-ton-years. The data sample used in this analysis is distinct from that of the Gd analysis, and the systematic uncertainties are also largely independent, with some exceptions, such as the reactor neutrino flux prediction. A combined rate- and energy-dependent fit finds $\sin^2 2\theta_{13} = 0.097 \pm 0.034\,(\text{stat.}) \pm 0.034\,(\text{syst.})$, excluding the no-oscillation hypothesis at $2.0\,\sigma$. This result is consistent with previous measurements of $\sin^2 2\theta_{13}$.

Neutrino oscillations are well established in the three flavor paradigm and can be described by three mixing angles (θ_{12}, θ_{23}, θ_{13}), a CP-violating phase δ, and two mass-squared differences (Δm_{21}^2, Δm_{32}^2). Among the three mixing angles, θ_{13} is the smallest and has recently been revealed to be non-zero [1, 2, 3, 4, 5, 6, 7]. The value of θ_{13} is a critical input for plans to measure δ and the neutrino mass hierarchy. Furthermore, it may provide important clues for physics beyond the Standard Model. The current best measurements of θ_{13} come from the reactor $\bar{\nu}_e$-disappearance experiments Double Chooz, Daya Bay, and RENO [6, 7, 5]. All three experiments rely on the detection of the inverse beta decay (IBD) interaction, $\bar{\nu}_e + p \rightarrow e^+ + n$, in Gd-doped liquid scintillator (LS). Typically these experiments search for a prompt positron signal followed by an ~ 8 MeV gamma cascade from neutron capture on Gd. Background due to natural radioactivity, which is predominantly below 4 MeV, is largely suppressed. However, in Double Chooz it is also possible to search for a prompt positron followed by a 2.2 MeV gamma ray from neutron capture on hydrogen, thanks to the low background environment in the detector.

Though the latter analysis presents several challenges, it provides important benefits: a cross-check on the standard Gd analysis and improved $\bar{\nu}_e$ energy spectrum shape information which is essential to our knowledge of θ_{13}.

In this letter we present an analysis of IBD interactions with neutron capture on hydrogen in the Double Chooz far detector. Following the same approach as in previous reports [3, 6], this analysis compares the candidate event rate and prompt energy spectrum shape to the Monte Carlo (MC) prediction. This analysis, however, differs from those reported [3, 6] in two major ways. First, the definition of the delayed signal is changed from the ~ 8 MeV gamma cascade characteristic of a neutron capture on Gd to the 2.2 MeV gamma ray characteristic of a neutron capture on hydrogen. This change allows us to select a data set that is statistically independent of the Gd-based data set and has different systematic uncertainties and background characteristics. Second, because hydrogen captures occur in the undoped LS in addition to the Gd-doped region, a three times larger fiducial volume is available for analysis.

The Double Chooz far detector is located at a distance of ~ 1050 m from the two $4.25\,\text{GW}_{\text{th}}$ reactor cores of the Chooz Nuclear Power Plant, with a rock overburden of 300 meters water equivalent. The central region of the detector consists of three concentric cylinders, collectively called the inner detector (ID). The innermost cylinder is the 10.3 m³ target. This is surrounded by a γ-catcher (22.5 m³). The target liquid is a PXE-based LS doped with Gd at a concentration of 1 g/l [8], while the γ-catcher liquid is an undoped LS. Outside the γ-catcher is the buffer, a 105 cm thick layer of non-scintillating mineral oil contained in a stainless steel tank. Light from the target and γ-catcher volumes is collected by 390 low-background 10-inch PMTs installed on the inner wall of the buffer tank [9, 10, 11]. Outside the buffer tank, and optically isolated from it, is the inner veto (IV), a 50 cm thick layer of liquid scintillator in a steel tank. The IV is equipped with 78 8-inch PMTs and serves as a veto for cosmic rays and fast neutrons entering the detector. The IV is surrounded by a 15 cm thick layer of demagnetized steel which suppresses γ-rays from radioactivity in the surrounding rock. Above the IV is the outer veto (OV) detector, a scintillator-strip-based muon tracking system. The OV system was installed during the data taking period, and about 2/3 of the data in this analysis benefit from OV use. A more detailed description of the entire detector can be found in Ref. [6].

The number of protons is estimated to be $(6.747 \pm 0.020) \times 10^{29}$ in the target [6] and $(1.582 \pm 0.016) \times 10^{30}$ in the γ-catcher volume, the latter being based on a geometrical survey and measurements of the scintillator hydrogen fraction.

The IBD signal is a twofold coincidence of a prompt positron energy deposition, E_{prompt}, and a delayed gamma energy deposition, E_{delay}, resulting from a neutron capture on hydrogen or Gd. The separation in time and space, Δt and Δr, of the coincident events are determined by neutron capture physics. Neutron capture times are 200 μs in the γ-catcher and 30 μs in the target, where the presence of Gd greatly increases the neutron capture probability. In this analysis, where we search for $E_{\text{delay}} \approx 2.2$ MeV without any fiducial volume cuts, we expect to detect candidates in both the target and γ-catcher. Given that only 13 % of the IBD interactions in the target volume are followed by neutron capture on hydrogen [6], 95 % of the signal events used in this analysis are located in the γ-catcher.

Vertex reconstruction is based on a likelihood maximiza-

tion of the charge and timing of the pulses detected at each PMT [6]. It allows the spatial correlation of prompt and delayed events, effectively removing accidental backgrounds.

We reconstruct the energy of all events via two steps: (1) a total charge (Q_{tot}) to photoelectron (PE_{tot}) conversion; and (2) a PE_{tot} to visible energy (E_{vis}) conversion as done in the Gd analysis [6]. The first step takes into account a channel-by-channel, non-linear gain calibration. The second step uses a light yield of ~ 230 PE/MeV, defined by the neutron capture peak on hydrogen in ^{252}Cf calibration source data. By applying correction factors derived from spallation neutron data, this step also corrects for the time variation and vertex dependence of the detector response. The same method is used to determine E_{vis} for the MC sample.

This analysis uses data collected by the Double Chooz far detector between April 13, 2011 and March 15, 2012, which is the same time-period used in the latest Double Chooz Gd analysis [6]. The total live time is 240.1 days, which is different from 227.9 days used in the Gd analysis [6] because of different analysis cuts.

The IBD candidate selection is performed via the following procedure. To reduce muon-induced backgrounds, we reject all events that occur less than 1 ms after a cosmic muon crosses the IV or the ID. We use PMT charge isotropy and PMT pulse simultaneity cuts to reduce backgrounds caused by light emitted from PMT bases ("light noise") [3]. We apply the following coincident selection cuts to the remaining events: 0.7 MeV < E_{prompt} < 12.2 MeV; 1.5 MeV < E_{delay} < 3.0 MeV; 10 μs < Δt < 600 μs; Δr < 90 cm. Furthermore, we reject prompt candidates that are coincident with a signal detected in the OV. This veto, along with the 10 μs lower bound of the Δt cut, renders backgrounds due to stopped muons negligible. Finally, we apply a multiplicity cut to reduce fast neutron backgrounds. This cut demands that no trigger occur in the 600 μs preceding the prompt candidate and that no trigger other than the delayed candidate occur in the 1000 μs following the prompt candidate.

The selection cuts yield a total of 36284 events. Among these IBD candidates are backgrounds due to uncorrelated accidental coincidences, fast neutrons produced by muons traversing the nearby rock, long-lived cosmogenic isotopes (mainly ^{9}Li), and a small contribution from light noise. Accidentals are the dominant background, comprising almost half the IBD candidate sample.

We measure the rate and energy spectrum of accidentals by analyzing a sample of off-time coincidences. We collect this sample by looking for a delayed trigger between 1 s + 10 μs and 1 s + 600 μs after a prompt candidate event and applying a multiplicity cut for a period of 1 s − 600 μs to 1 s + 1000 μs. To increase sample statistics, we open 124 consecutive windows after this first window, thus sampling accidentals between 1 s and 1.2 s after each prompt candidate. After correcting for inefficiencies associated with this selection method, we obtain an accidentals rate of

73.45 ± 0.16 events/day. The result is cross-checked among multiple independent methods, and the quoted value includes the largest systematic uncertainty among them.

The fast neutron background consists of a proton recoil, the prompt event, in coincidence with the capture of the neutron, the delayed event. A single muon passing close to the detector may generate one or more fast neutrons which traverse the IV and ID. We tag the number of IBD candidates in which fast neutrons are recorded simultaneously in the IV and ID by requiring $\geq$ 2 IV PMT hits and an ID-IV pulse-timing correlation. We estimate the tagging efficiency from an event sample with E_{prompt} > 12 MeV, following the same method as used for the Gd analysis [6]. From this sample we obtain a spectrum shape and, using the tagging efficiency and sample purity, we calculate the fast neutron rate to be 2.50 ± 0.47 events/day.

Muon-induced radioactive isotopes which emit a neutron immediately following β-decay, such as ^{9}Li, can be a background to IBD reactions. As the lifetime of ^{9}Li is 257 ms, we use the correlation of the ^{9}Li decay events to previously detected muons to estimate the ^{9}Li background rate. To increase the purity of ^{9}Li in our sample, we consider only the subset of IBD candidates for which the spatial separation between the prompt event and the reconstructed muon track is within a defined distance. While ID PMTs are used to reconstruct the muon tracks in the Gd analysis [6], IV PMTs are used in this analysis to account for muons going through non-scintillating buffer liquid. To estimate the ^{9}Li rate in this subsample, we fit the time difference Δt_μ between the IBD candidate prompt events and preceding muons with an exponential function characterized by the ^{9}Li lifetime, plus a flat function to accommodate remaining accidentals and IBD candidates. The estimated rate is found to be consistent with that in the Gd analysis [6], accounting for the different fiducial volumes and selection efficiencies, and the difference is included in the systematic uncertainty. We find a ^{9}Li rate of 2.8 ± 1.2 events/day. Muon track reconstruction efficiency is evaluated by a MC study and added into the systematic uncertainty. We estimate the shape and associated systematic uncertainty from MC, as was done in the Gd analysis [6].

Finally, we found a small number of light noise events creating two consecutive triggers that are identified as IBD candidates. A volume cut on the reconstructed vertex is used to quantify the rate and E_{prompt} spectrum shape for this type of background. We estimate this background rate as 0.32 ± 0.07 events/day.

In this analysis, neutron detection efficiency ϵ_n includes both the efficiency of the IBD selection and the fraction of neutron captures which occur on hydrogen. We evaluate ϵ_n from ^{252}Cf neutron source calibration data and find it to be $\epsilon_n = 0.0846 \pm 0.0018$ in the target and $\epsilon_n = 0.7853 \pm 0.0036$ in the γ-catcher. Weighting by the fraction of predicted IBD candidates in each region, we estimate the uncertainty in the detection efficiency over the entire fiducial volume as 1.0 %. Finally, we find that
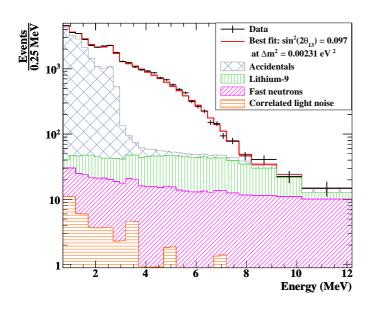
Figure 1: (Color online) Stacked histogram showing the prompt energy spectrum of neutrino candidates without background subtraction (black data points with statistical error bars). The red (grey) line is the best fit oscillation hypothesis. Also shown are contributions from accidentals (blue cross-hatched), ^{9}Li (green vertical lines), fast neutrons (purple diagonal lines), and correlated light noise (orange horizontal lines).

Table 1: Summary of the number of observed IBD candidates and the predictions for the signal and background contributions used as input for the oscillation fit analysis.

Source	Predicted/observed events
$\bar{\nu}_e$ prediction (no osc.)	17690
Accidentals	17630
Cosmogenic isotopes	680
Fast neutrons	600
Light noise	80
Total prediction	36680
Observed IBD candidates	36284

Table 2: Summary of signal and background normalization uncertainties relative to the predicted signal.

Source	Uncertainty [%]
Reactor flux	1.8
Statistics	1.1
Accidental background	0.2
Cosmogenic isotope background	1.6
Fast neutrons	0.6
Light noise	0.1
Energy scale	0.3
Efficiency	1.6
Total	3.1

an uncertainty of 1.2 % accounts for the MC modeling of neutron migration, called spill-in/out [6], between detector subvolumes. Adding these factors in quadrature, we obtain a total detection efficiency uncertainty of 1.6 %.

Energy scale uncertainty arises from three sources: time variation, non-linearity, and non-uniformity in the detector response. We treat the first two effects exactly as in Gd analysis [6]. The third effect has a larger impact on the hydrogen analysis because of its extended fiducial volume. We estimate it by comparing data and MC from calibration source deployments in the γ-catcher. In total, we find an energy scale uncertainty of 1.7 %, as compared to 1.1 % used in the Gd analysis [6].

The reference E_{prompt} spectrum is selected from the same reactor power-based $\bar{\nu}_e$ MC sample generated for the Gd analysis [6]. Systematic uncertainties on the reference spectrum are the same as for the Gd analysis. We use the Bugey4 measurement to minimize the systematic uncertainty on the reactor neutrino flux prediction [12, 6], which is the dominant uncertainty in this analysis. The no-oscillation expectation for the number of neutrino candidates is 36680 ± 520, including background. The predicted number of events for both signal and backgrounds are summarized in Tab. 1, and uncertainties relative to the predicted signal statistics are shown in Tab. 2.

To extract $\sin^2 2\theta_{13}$ we compare both the rate and shape of the data to the reference E_{prompt} spectrum in 31 variably sized energy bins from 0.7 to 12.2 MeV. The fit procedure is identical to that used in the Gd analysis [3, 6], except that we use a single integration period and include the Δr cut efficiency as an additional source of uncertainty. We use the MINOS value of $\Delta m^2 = (2.32 \pm 0.12) \times 10^{-3} \text{eV}^2$ as input for the fit [13]. We find a best fit of

$$\sin^2 2\theta_{13} = 0.097 \pm 0.034 \, (\text{stat.}) \pm 0.034 \, (\text{syst.})$$

with χ^2/DOF of 38.9/30. As in the Gd analysis [6], we define statistical error as the portion of the 1 σ error which can be improved by collecting more data. This includes uncertainty from our current statistics (see Tab. 2) and uncertainty on background shapes. We define systematic error as the uncertainty which cannot be reduced simply by collecting more data. Figure 1 shows the com-
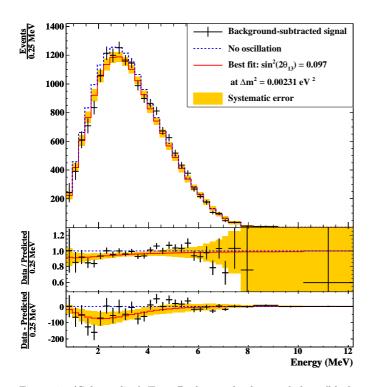
Table 3: Summary of pull parameters in the oscillation fit. The input values are determined by measurements, and the best-fit values are outcome of oscillation fit.

Pull parameter	Initial value	Best-fit value
Cosmogenic isotope [day^{-1}]	2.8 ± 1.2	3.9 ± 0.6
Fast neutrons [day^{-1}]	2.5 ± 0.5	2.6 ± 0.4
Energy scale	1.00 ± 0.02	0.99 ± 0.01
$\Delta m^2 (10^{-3}\mathrm{eV}^2)$	2.32 ± 0.12	2.31 ± 0.12

Figure 2: (Color online) Top: Background-subtracted data (black points with statistical error bars) are superimposed on the prompt energy spectra expected in the case of no oscillations (dashed blue line) and for our best fit $\sin^2 2\theta_{13}$ (solid red line). The best fit has χ^2/DOF of 38.9/30. Solid gold bands indicate systematic errors in each bin. Middle: The ratio of data to the no-oscillation prediction (black points with statistical error bars) is superimposed on the expected ratio in the case of no oscillations (blue dashed line) and for our best fit $\sin^2 2\theta_{13}$ (solid red line). Gold bands indicate systematic errors in each bin. Bottom: The difference between data and the no-oscillation prediction is shown in the same style as the ratio (above).

plete spectrum of IBD candidates with the fitted background contributions, while Fig. 2 shows the background-subtracted E_{prompt} spectrum along with the best fit. The pull parameters from the fit are summarized in Tab. 3 together with the input values. We have performed a frequentist study to determine the compatibility of the data and the no-oscillation hypothesis. Based on a $\Delta\chi^2$ statistic, defined as the difference between the χ^2 at the best fit and at $\sin^2 2\theta_{13} = 0$, the data exclude the no-oscillation hypothesis at 97.4% $(2.0\,\sigma)$. A fit incorporating only the rate information yields $\sin^2 2\theta_{13} = 0.044 \pm 0.022\,(\mathrm{stat.}) \pm 0.056\,(\mathrm{syst.})$. A simple ratio of observed to expected signal statistics yields R $= 0.978 \pm 0.011\,(\mathrm{stat.}) \pm 0.029\,(\mathrm{syst.})$ at the far site.

The smaller best-fit value of $\sin^2 2\theta_{13}$ by the rate-only analysis can be explained by the ^{9}Li background. The fit to the energy spectrum indicates a larger ^{9}Li background contamination than the original estimate, although it is consistent within the systematic uncertainty.

In summary, due to the low level of backgrounds achieved in the Double Chooz detector, we have made the first measurement of $\sin^2 2\theta_{13}$ using the capture of IBD neutrons on hydrogen. This technique enabled us to use a different data set with partially different systematic uncertainties than that used in the standard Gd analysis [6]. An analysis based on rate and spectral shape information yields $\sin^2 2\theta_{13} = 0.097 \pm 0.034\,(\mathrm{stat.}) \pm 0.034\,(\mathrm{syst.})$, which is in good agreement with the result of the Gd analysis $\sin^2 2\theta_{13} = 0.109 \pm 0.030\,(\mathrm{stat.}) \pm 0.025\,(\mathrm{syst.})$ [6]. With increased statistics and a precise evaluation of the correlation of the systematic uncertainties, a combination of the two results is foreseen for the future.

References

[1] K. Abe *et al. Phys. Rev. Lett.*, 107 041801 (2011).
[2] P. Adamson *et al. Phys. Rev. Lett.*, 107, 181802 (2011).
[3] Y. Abe *et al. Phys. Rev. Lett.*, 108, 131801 (2012).
[4] F.P. An *et al. Phys. Rev. Lett.*, 108, 171803 (2012).
[5] J.K. Ahn *et al. Phys. Rev. Lett.*, 108, 191802 (2012).
[6] Y. Abe *et al. Phys. Rev. D*, 86, 052008 (2012).
[7] F.P. An *et al. Chinese Physics C*, 37, 011001 (2013).
[8] C. Aberle *et al. JINST*, 7, P06008 (2012).
[9] E. Calvo *et al. NIM A*, 621, 222 (2010).
[10] C. Bauer *et al. JINST*, 6, P06008 (2011).
[11] T. Matsubara *et al. NIM A*, 661, 16 (2012).
[12] Y. Declais *et al. Phys. Lett. B*, 338, 383 (1994).
[13] P. Adamson *et al. Phys. Rev. Lett.*, 106, 181801 (2011).